Short Article

Molecular Cell

MICU1 Interacts with the D-Ring of the MCU Pore to Control Its Ca^{2+} Flux and Sensitivity to Ru360

Graphical Abstract

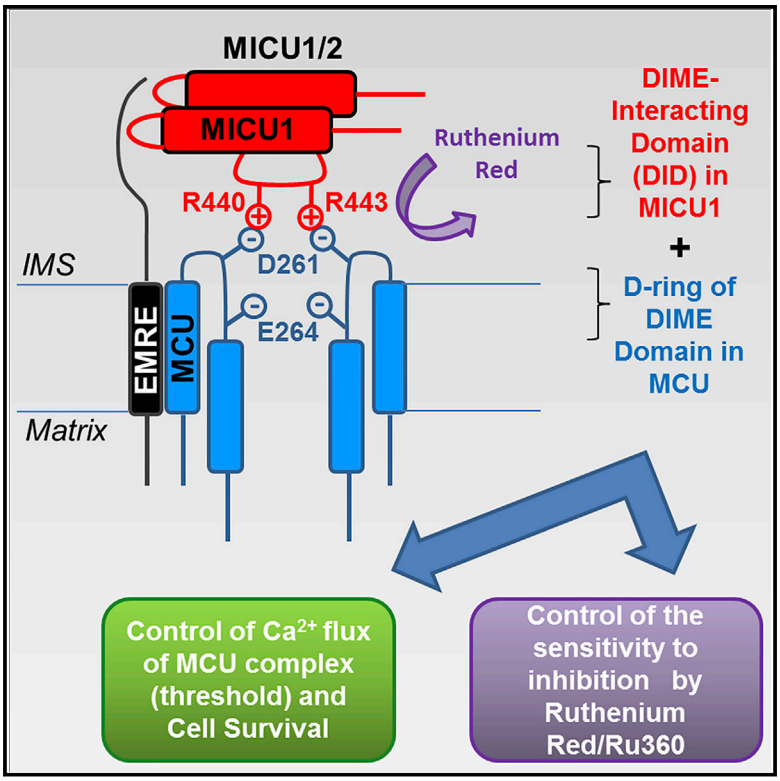

Highlights

- MICU1 controls the RuRed/Ru360 sensitivity of the MCU complex
- MICU1's R440/443 supports a direct interaction with MCU
- MICU1 R440/443-dependently competes with RuRed for interacting with the D-ring of MCU
- MICU1-MCU interaction is central for MCU gatekeeping and cell survival

Authors

Melanie Paillard, György Csordás, Kai-Ting Huang, Peter Várnai, Suresh K. Joseph, György Hajnóczky

Correspondence

gyorgy.hajnoczky@jefferson.edu

In Brief

Paillard et al. report that mitochondrial Ca^{2+} uptake 1 (MICU1) interacts with the D-ring of MCU, the pore-forming protein of the mitochondrial Ca^{2+} uniporter, through a DIME interacting domain involving the arginines 440 and 443 to control both the Ca^{2+} flux and the ruthenium red sensitivity of the MCU complex.

Paillard et al., 2018, Molecular Cell 72, 778–785
November 15, 2018
https://doi.org/10.1016/j.molcel.2018.09.008

CellPress

CellPress

Molecular Cell
Short Article

MICU1 Interacts with the D-Ring of the MCU Pore to Control Its Ca^{2+} Flux and Sensitivity to Ru360

Melanie Paillard,[1] György Csordás,[1] Kai-Ting Huang,[1] Peter Várnai,[2] Suresh K. Joseph,[1] and György Hajnóczky[1,3,*]
[1]MitoCare Center, Department of Pathology, Anatomy and Cell Biology, Thomas Jefferson University, Philadelphia, PA 19107, USA
[2]Department of Physiology, Semmelweis University, Budapest, 1094 Hungary
[3]Lead Contact
*Correspondence: gyorgy.hajnoczky@jefferson.edu
https://doi.org/10.1016/j.molcel.2018.09.008

SUMMARY

Proper control of the mitochondrial Ca^{2+} uniporter's pore (MCU) is required to allow Ca^{2+}-dependent activation of oxidative metabolism and to avoid mitochondrial Ca^{2+} overload and cell death. The MCU's gatekeeping and cooperative activation is mediated by the Ca^{2+}-sensing MICU1 protein, which has been proposed to form dimeric complexes anchored to the EMRE scaffold of MCU. We unexpectedly find that MICU1 suppresses inhibition of MCU by ruthenium red/Ru360, which bind to MCU's DIME motif, the selectivity filter. This led us to recognize in MICU1's sequence a putative DIME interacting domain (DID), which is required for both gatekeeping and cooperative activation of MCU and for cell survival. Thus, we propose that MICU1 has to interact with the D-ring formed by the DIME domains in MCU to control the uniporter.

INTRODUCTION

The mitochondrial Ca^{2+} uniporter (mtCU) or MCU complex needs to be tightly regulated to avoid cell death by Ca^{2+} overload and to allow the Ca^{2+}-dependent physiological stimulation of oxidative metabolism. Among the different components of the MCU complex, the Ca^{2+}-sensing protein MICU1 has been characterized as a key mediator of gatekeeping and cooperative activation of MCU, the pore-forming unit of the MCU complex (Csordás et al., 2013; Kamer and Mootha, 2014; Mallilankaraman et al., 2012; Patron et al., 2014). MICU1 has been linked to human neurological and muscular diseases (Lewis-Smith et al., 2016; Logan et al., 2014), as well as to liver regeneration (Antony et al., 2016), cardiac ischemia-reperfusion injury (Xue et al., 2017), diabetic cardiomyopathy (Ji et al., 2017) and ovarian cancer (Chakraborty et al., 2017).

In addition to MCU and MICU1, other MCU complex components have also been identified: two paralogs of MICU1, MICU2 and MICU3 (Plovanich et al., 2013), a dominant-negative paralog of MCU, MCUb (Raffaello et al., 2013), and the indispensable transmembrane protein EMRE (Sancak et al., 2013). MICU1 interacts with MICU2 through a disulfide bond involving C465 in MICU1 and C410 in MICU2 to form homo/heterodimers that control the MCU complex activity (Patron et al., 2014; Petrungaro et al., 2015). On the other hand, MICU1 binding to the polyaspartate tail of EMRE has been shown to anchor MICU1 to the MCU complex in the mitochondrial intermembrane space and thus confer gatekeeping of the pore (Tsai et al., 2016). However, in the same study, MICU1's interaction with MCU without EMRE was also shown by coimmunoprecipitation (Tsai et al., 2016), which is also supported by surface plasmon resonance data (Vecellio Reane et al., 2016).

Topology studies showed that most of MCU's amino acid residues are in the two transmembrane domains and the N and C termini that are exposed to the mitochondrial matrix and identified a short sequence between the two transmembrane domains, which is exposed to the intermembrane space (IMS) and might be accessible for direct interaction with IMS proteins like MICU1. This motif was termed as DIME (or DXXE) based on its amino acid sequence conserved across species (D261 and E264 in hsMCU) (Baughman et al., 2011). A recent study characterized the DIME domain as the ion selectivity filter of the MCU with ion binding to the two carboxylate rings (Cao et al., 2017). Notably, mutation of DIME domain also impaired the MICU1-MCU interaction (Patron et al., 2014). Interestingly, the inhibitory effect of the most potent inhibitors of the MCU complex, ruthenium red (RuRed) and ruthenium 360 (Ru360), requires S259 (Baughman et al., 2011). Two recent NMR studies further indicated that Ru360/RuRed binds the D-ring of MCU's selectivity filter, which is solvent-exposed compared to the E-ring located deeper in the pore (Arduino et al., 2017; Cao et al., 2017). Thus, we reasoned that MICU1 might affect the RuRed sensitivity of the MCU complex through a potential interaction with the DIME domain of MCU.

We here find that MICU1 deletion increases the MCU complex sensitivity to RuRed/Ru360, suggesting that MICU1 interferes with the binding site of these inhibitors in the DIME motif of MCU. We then identify a complementing sequence in MICU1 to the DIME motif, which we refer to as DIME interacting domain (DID) and predict that two arginines (R440 and R443) engage in potential salt bridges with the D-ring of MCU. Using an imaging approach to assess both threshold and cooperativity of the MCU complex in MICU1-KO mouse embryonic fibroblasts (MEFs) and HEK293 cells (HEKs), we show that the DID in MICU1 is required to control the MCU complex-mediated Ca^{2+} influx and, in turn,

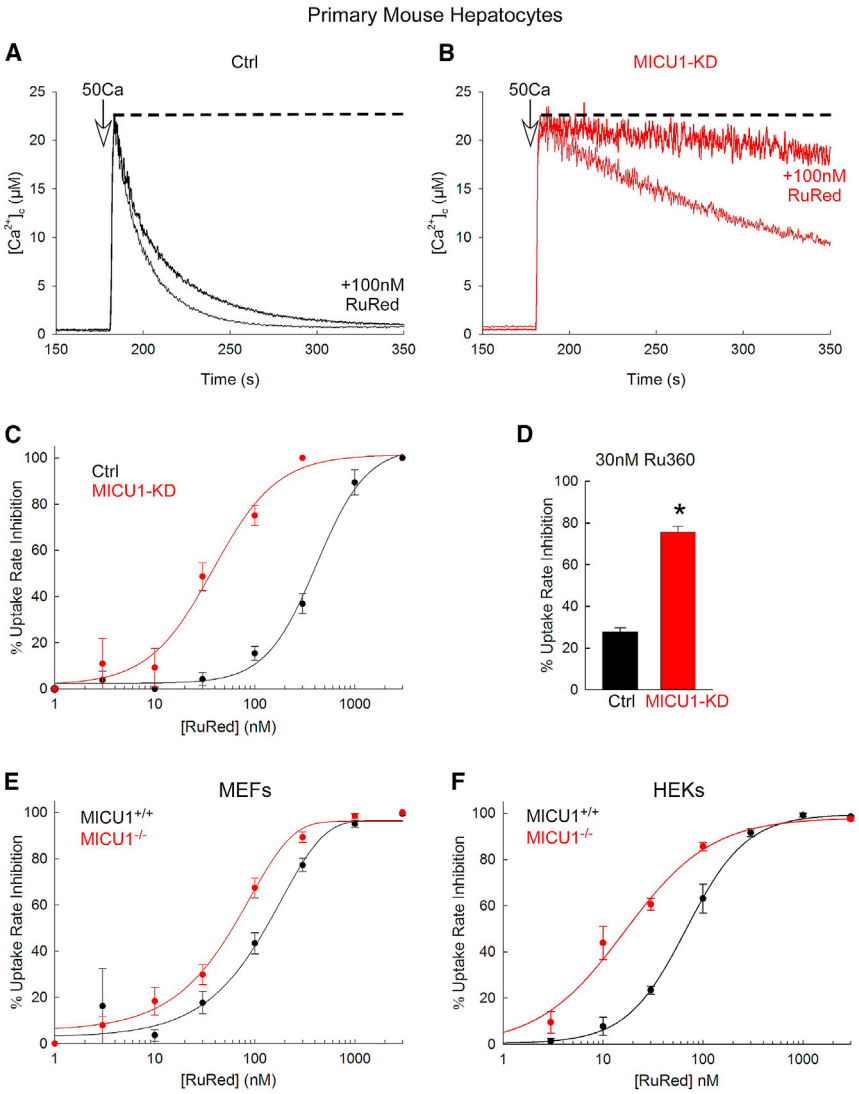

Figure 1. MICU1 Controls the RuRed/Ru360 Sensitivity of MCU Complex

(A and B) Time courses of the mitochondrial clearance of the $[Ca^{2+}]_c$ rise upon addition of a 50 μM $CaCl_2$ bolus (50Ca) in permeabilized Ctrl (A) and MICU1-KD hepatocytes (B), with and without 100 nM RuRed. Dashed line indicates complete inhibition of the mitochondrial Ca^{2+} uptake.

(C) [RuRed] dose response for the percentage of inhibition of the initial mitochondrial uptake rate for a 50Ca bolus in Ctrl (black) and MICU1-KD (red) hepatocytes. A sigmoidal fit is displayed for each.

(D) Percentage of uptake rate inhibition by 30 nM Ru360 in Ctrl (black) and MICU1-KD (red) hepatocytes.

(E and F) [RuRed] dose response for the percentage of uptake rate inhibition for a 20Ca bolus in $MICU1^{+/+}$ and $MICU1^{-/-}$ MEFs (E) and HEKs (F). A sigmoidal fit is displayed for each.

Mean ± SEM, n = 3–4, *p < 0.05 versus Ctrl, t test. See also Figure S1.

cell survival. Finally, we show that the DID of MICU1 alters the RuRed/Ru360 sensitivity by competing for the interaction with the DIME domain of MCU, thus opening a new avenue for therapeutic targeting of the MCU complex.

RESULTS

MICU1 Controls the RuRed/Ru360 Sensitivity of the MCU Complex

While recording mitochondrial clearance of Ca^{2+} added to the cytoplasmic buffer of permeabilized hepatocytes isolated from wild-type (Ctrl) and hepatocyte-specific $MICU1^{-/-}$ mouse (MICU1-KD), we noticed that deletion of MICU1 caused sensitization to RuRed (Figures 1A and 1B). Specifically, MICU1-deficient mitochondria showed less-effective uptake when a large Ca^{2+} bolus was applied (50 μM $CaCl_2$) as we reported earlier (Antony et al., 2016), and it was almost completely suppressed by a submaximal dose of RuRed (100 nM), which caused only a small inhibition in wild-type (WT) mitochondria. When dose response curves were compiled, an increase in sensitivity for RuRed of almost an order of magnitude was observed in MICU1-deficient hepatocytes (Figure 1C). Higher sensitivity to RuRed was also observed in MICU1-deficient hepatocytes in response to a smaller bolus of Ca^{2+} (7 μM; raising $[Ca^{2+}]_c$ to 1.5–2 μM) (Figure S1), for which the mitochondrial Ca^{2+} uptake is similar to the control (Antony et al., 2016). The sensitivity was also increased toward Ru360, which is a more specific inhibitor of MCU complex (Figure 1D). Furthermore, sensitization to RuRed by MICU1 deletion was also found in MEFs (Figure 1E) and in HEKs (Figure 1F). Thus, these results provide evidence that MICU1 decreases the RuRed/Ru360 sensitivity of the MCU complex, probably by competing with RuRed/Ru360 for binding to MCU.

MICU1 Has a Complementing Sequence to the Region of MCU Determining RuRed Sensitivity and Ca^{2+} Selectivity

RuRed/Ru360 was recently shown to bind the DIME domain of MCU (Arduino et al., 2017; Baughman et al., 2011; Cao et al., 2017). The results shown in Figure 1 led us to postulate that there might be a domain in MICU1 that interacts with the DIME domain of MCU. It has been previously suggested that MICU1 interacts indirectly with MCU through EMRE, involving the transmembrane domains of MCU and EMRE, and EMRE binding to MICU1 via EMRE's C-terminal polyaspartate tail (Sancak et al., 2013; Tsai et al., 2016). Nevertheless, two studies using different techniques have indicated that MICU1 can interact with MCU without EMRE (Tsai et al., 2016; Vecellio Reane et al., 2016), supporting the possibility of an additional protein-protein interaction component. Moreover, along with the DIME domain of MCU (Patron et al., 2014), the C-terminal structure of MICU1 has been

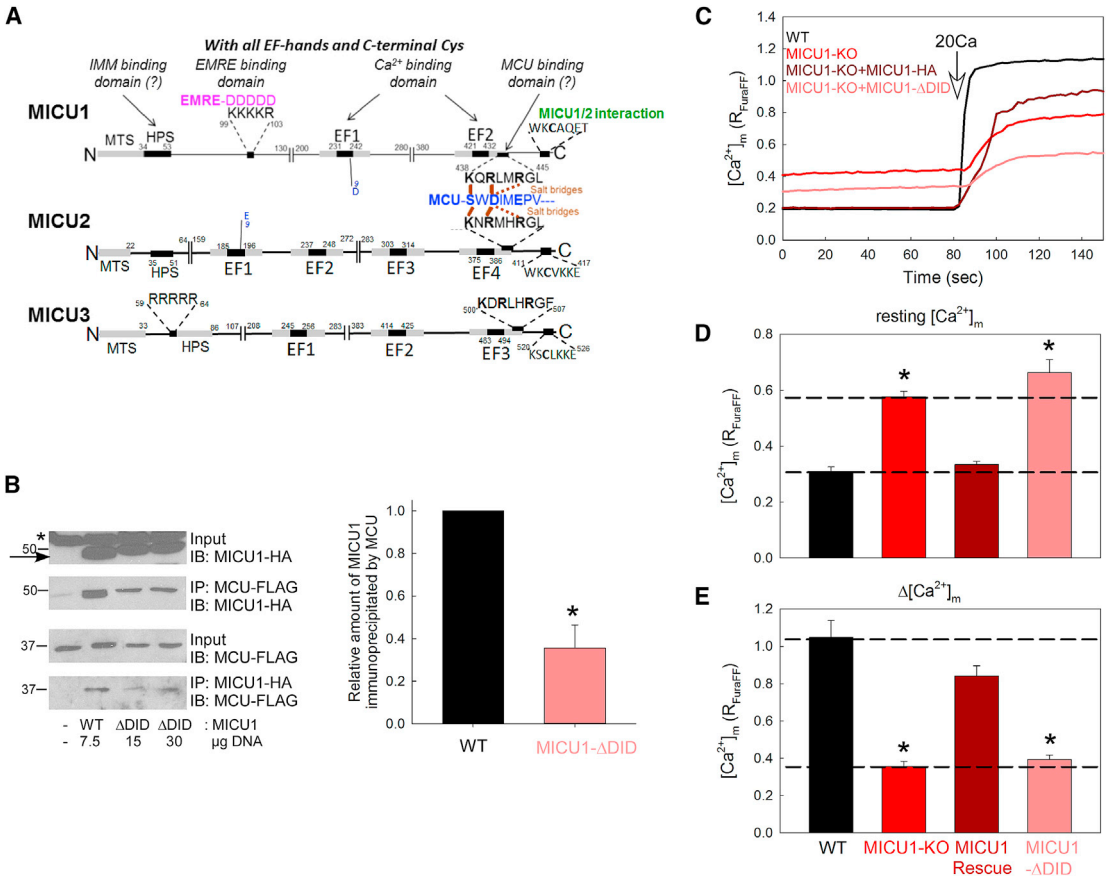

Figure 2. Mutation of the Complementing Sequence Interferes with MICU1 Binding to and Control of MCU

(A) Alignment of MICU1, MICU2 and MICU3 showing previously identified sites in MICU1 involved in interactions with EMRE and MICU1/MICU2, and proposing a potential MCU binding domain.

(B) Upper: representative immunoblotting of coimmunoprecipitation (coIP) between MCU-FLAG and HA-tagged WT MICU1 or MICU1-ΔDID mutant expressed in MCU-FLAG HEKs. Arrow indicates specific MICU1-HA band, while asterisk is an unspecific band. Lower: quantification of the relative MICU1 amount pulled down by MCU-FLAG in HEKs expressing WT MICU1 or MICU1-ΔDID. Mean ± SEM, n = 3, *p < 0.05 versus WT, t test.

(C) $[Ca^{2+}]_m$ measurements in permeabilized WT MEFs and MICU1-KO MEFs expressing empty vector, MICU1 or MICU1-ΔDID and challenged with a bolus of 20 μM $CaCl_2$.

(D) Quantification of resting $[Ca^{2+}]_m$ as an index of thresholding of the MCU complex.

(E) Calculations of the difference ($\Delta[Ca^{2+}]_m$) between the $[Ca^{2+}]_m$ 30 s post-20Ca addition and the resting $[Ca^{2+}]_m$ as an index of cooperativity of the MCU complex. Mean ± SEM, n = 6, *p < 0.05 versus WT, one-way ANOVA.

See also Figure S2.

shown to be necessary for co-immunoprecipitation with MCU (Kamer and Mootha, 2014; Wang et al., 2014). However, the exact sequence in MICU1 involved in the binding to MCU is still unknown. Alignment of MICU1, MICU2, and MICU3 revealed a potential DIME interacting domain in the C-terminal sequence of all three MICUs, involving lysine (K438) and two arginines (R440 and R443), which could form potential salt bridges with the DIME domain in MCU (Figure 2A). Among the marked potential interactions, the one between K438 and the corresponding serine is more likely a dipole-dipole interaction than an actual salt bridge between the positively charged amino group of lysine and the OH of serine. The crystal structure of MICU1 shows that the two arginine residues are orientated in the same direction in a helix (Wang et al., 2014), thus suggesting that the side chains of R440 and R443 could act like RuRed to bind to the outer D-ring of the pore of the MCU pentamer (Cao et al., 2017). To validate our hypothesis, we mutated in hsMICU1 these 3 residues to alanine (MICU1-ΔDID: 440KQRLMR445 > 440AQALMA445) and analyzed its binding with MCU. MICU1-ΔDID (tagged with HA) was pulled down 60% less than WT MICU1 by MCU (tagged with FLAG), and MCU was pulled down to a lesser extent by MICU1-ΔDID than by WT MICU1 (Figure 2B). These results suggest that the KQRLMR sequence in MICU1, which we now named DID (DIME interaction domain), interacts with MCU, probably through its DIME motif.

Next, using MICU1-KO MEFs, in which MICU2 is maintained (Antony et al., 2016), we aimed at better characterizing the functional role of the DID in MICU1 in the control of the MCU complex Ca^{2+} flux. To assess MCU complex activity in individual cells, $[Ca^{2+}]_m$ was followed via loading the mitochondria in WT and

MICU1-KO MEF cells with the ratiometric probe furaFF/AM; cells were then permeabilized and subjected to a two-step Ca^{2+} addition protocol (3 and 20 μM $CaCl_2$, 3 and 20Ca). Mitochondrial localization of the probe was confirmed by complete inhibition of the Ca^{2+} response by RuRed (Figure S2) (Paillard et al., 2017). As expected, MICU1-KO MEFs displayed an increased resting $[Ca^{2+}]_m$, which could be prevented by RuRed (Figure S2). The resting $[Ca^{2+}]_m$ was used then as a measure of gatekeeping activity of various MICU1 mutants. Rescue was performed with WT MICU1 (MICU1-HA) or MICU1-ΔDID in the MICU1-KO cells. While MICU1-HA restored the low resting $[Ca^{2+}]_m$, MICU1-ΔDID failed to lower it (Figures 2C and 2D). As a simple measure of the Ca^{2+}-induced highly cooperative activation of MCU, in a single-addition protocol, the initial response to 20Ca (difference between the $[Ca^{2+}]_m$ 30 s post-20Ca addition and the resting $[Ca^{2+}]_m$) was used. MICU1-ΔDID expression decreased Δ $[Ca^{2+}]_m$ as in MICU1-KO MEFs (with empty vector), compared to WT MEFs (Figures 2C and 2E). Thus, our data support that mutation of the complementing sequence with MCU DIME motif interferes with MICU1 binding to and control of the Ca^{2+} fluxes of MCU.

Role of DID and the Other Motifs of MICU1 in Intracellular Ca^{2+} Homeostasis and Cell Survival

MICU1 is thus engaged in at least three interactions with components of the MCU complex: the previously documented dimerization with MICU2/MICU1, an interaction with EMRE, and our newly demonstrated interaction with MCU via the DID. To evaluate the MCU complex regulation by the interactions of MICU1 with MICU2, EMRE and MCU, respectively, we interfered with each separately or in combination and performed simultaneous $[Ca^{2+}]_c$ and $[Ca^{2+}]_m$ measurements during store-operated Ca^{2+} entry (SOCE) in intact WT and MICU1-KO HEKs. We opted for SOCE as the Ca^{2+} source because it stimulates mitochondrial Ca^{2+} uptake mostly via the global $[Ca^{2+}]_c$ increase that we measured, so we could plot $[Ca^{2+}]_m$ as both a function of time and $[Ca^{2+}]_c$. We generated three additional HA-tagged mutants of MICU1: the MICU1-Δdimer (C465A), which is incompetent for dimerization, MICU1-ΔEMRE (99KKKKR > 99AAAAA), which lacks the EMRE-binding motif, and a combination of MICU1-ΔDID+ΔEMRE+Δdimer. Co-transfection of MICU1-KO cells with MICU1 mutants and the mitochondrial matrix-targeted Ca^{2+} indicator, mtCepia, allowed us to evaluate in each single cell $[Ca^{2+}]_m$ and $[Ca^{2+}]_c$ by fura2 (Figures 3A and 3B). The SOCE-mediated $[Ca^{2+}]_m$ increase appeared earlier in MICU1-KO HEKs rescued by either the empty vector, the MICU1-ΔDID, or the MICU1-ΔDID+ΔEMRE+Δdimer mutant, compared to WT HEKs or MICU1-KO cells rescued by the other MICU1 mutants (Figure 3B). The $[Ca^{2+}]_m$ response 60 s post-Ca^{2+} addition revealed that both MICU1-ΔDID and MICU1-ΔDID+ΔEMRE+Δdimer mutant rescues took up Ca^{2+} similarly to the MICU1-KO cells, while the MICU1-ΔEMRE and MICU1-Δdimer rescued cells took up initially less Ca^{2+}, like the WT MICU1 rescue (Figure 3C). Plotting $[Ca^{2+}]_m$ against $[Ca^{2+}]_c$ further supported that MICU1-KO cells rescued by either the empty vector or the MICU1-ΔDID or the MICU1-ΔDID+ΔEMRE+Δdimer mutant showed a significant $[Ca^{2+}]_m$ increase at lower $[Ca^{2+}]_c$ than WT cells or the ones rescued by WT MICU1 and the other MICU1 mutants in MICU1-KO HEKs (Figure 3D). Indeed, to reach a similar level of $[Ca^{2+}]_m$ (arbitrarily set at 1.2 ratio units), around 0.2 μM of $[Ca^{2+}]_c$ was sufficient in MICU1-KO and the MICU1-ΔDID or MICU1-ΔDID+ΔEMRE+Δdimer rescues, whereas WT HEKs and MICU1-KO cells rescued by WT MICU1, MICU1-ΔEMRE, or MICU1-Δdimer constructs required a significantly higher $[Ca^{2+}]_c$ (Figure 3E). We further assessed if the MICU1-ΔDID mutant operated as a dominant-negative MCU complex component in these intact cell experiments. Similarly to MICU1-KO HEKs, co-expression of WT MICU1 and MICU1-ΔDID led to a significant $[Ca^{2+}]_m$ increase at lower $[Ca^{2+}]_c$ than MICU1-KO HEKs rescued by WT MICU1 itself or along with a point mutant in EF1 of MICU1 (MICU1-EF1-D9E), thus unraveling a dominant-negative effect of MICU1-ΔDID over WT MICU1 (Figures S3A and S3B). MICU1-EF1-D9E was created to cause a specific perturbation in D239 of the EF hand, but it was found to unalter the resting $[Ca^{2+}]_m$ or the rescue of cooperativity and Ca^{2+}-dependent activation of MCU complex (Figures S3C–S3E). Therefore, we used this construct as an alternative example of full rescue. Together, these data suggest that the MICU1-MCU interaction through the MICU1's DID and MCU's DIME motif is the most critical for the gatekeeping of the MCU complex.

Because the gatekeeping of MCU complex by MICU1 is central to avoiding mitochondrial Ca^{2+} overload, oxidative stress, and cell death (Antony et al., 2016; Csordás et al., 2013; Liu et al., 2016; Mallilankaraman et al., 2012), we then proceeded to study the so-called delayed Ca^{2+} dysregulation by following the $[Ca^{2+}]_c$ in intact HEKs subjected to prolonged Ca^{2+} entry (Figure 3F). After the initial $[Ca^{2+}]_c$ rise, a large delayed increase was observed only in mock- and MICU1-ΔDID-rescued cells, whereas $[Ca^{2+}]_c$ was maintained at a low level in MICU1-KO HEKs rescued by WT MICU1 or with the MICU1-EF1-D9E (Figure 3G).

The mitochondrial oxidative stress generated during prolonged SOCE conditions was measured using mtGrx1-RoGFP2, the fluorescence of which shows the ratio of oxidized and reduced glutathione (GSSG/GSH) and is unaffected by pH (Gutscher et al., 2008). The oxidative stress recorded in mock rescued cells was duplicated in the cells rescued by the MICU1-ΔDID mutant, whereas oxidative stress was avoided in the cells rescued with WT MICU1 or MICU1-EF1-D9E constructs (Figure 3H). Importantly, all the MICU1 constructs were effectively expressed in the MICU1-KO cells, with no difference between the MICU1-ΔDID and MICU1-EF1-D9E mutants (Figure S4A). To conclude, these results indicate that MICU1 interaction with the D-ring of the DIME domain of MCU is required for gatekeeping of the MCU complex and, in turn, for cell survival.

DID Mutant Fails to Rescue RuRed Sensitivity

Finally, we investigated how RuRed sensitivity will be altered with expression of DID mutant of MICU1. While in WT and in MICU1-KO HEKs rescued by WT MICU1, or MICU1-EF1-D9E constructs, 30 nM RuRed elicited a partial inhibition of the mitochondrial Ca^{2+} uptake rate, MICU1-KO HEKs rescued with empty vector or MICU1-ΔDID displayed an almost complete inhibition of mitochondrial Ca^{2+} uptake, which could only be attained with 3 μM RuRed in WT HEKs (Figures 4A and 4B). Indeed,

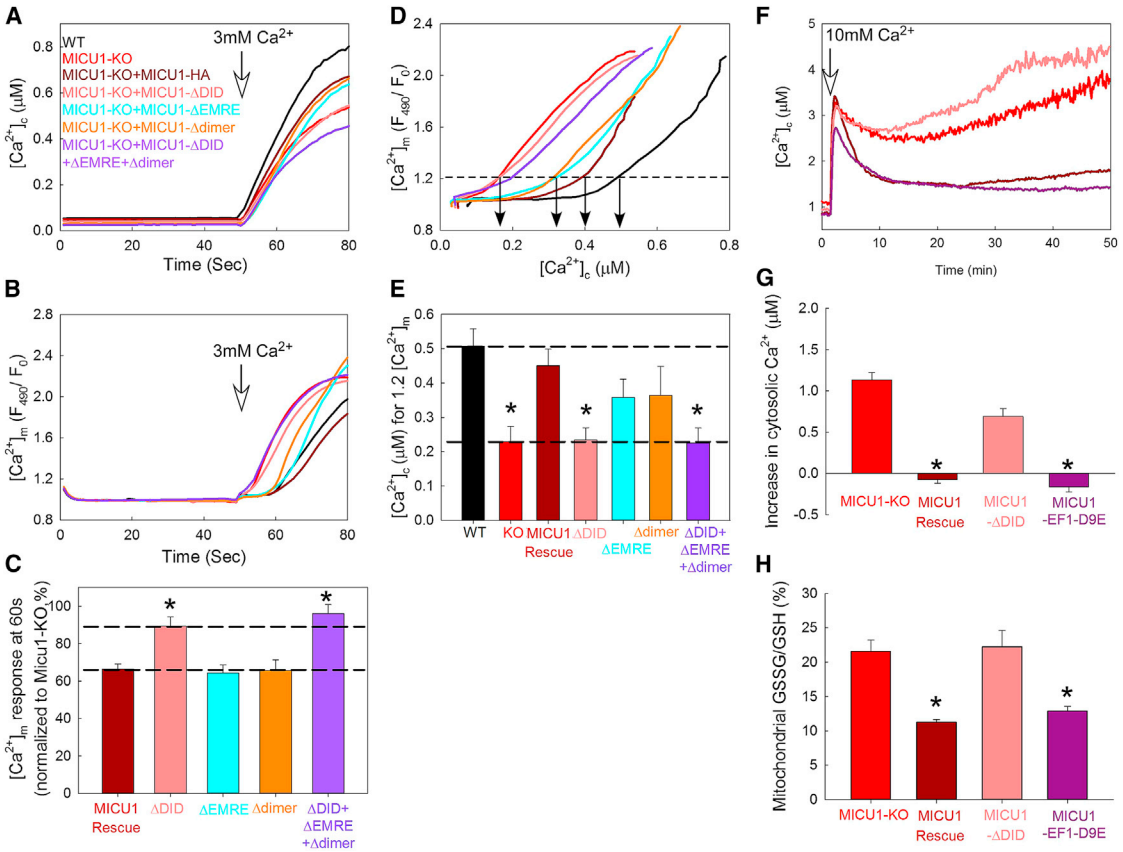

Figure 3. Critical Role of the DID of MICU1 in Ca^{2+} Homeostasis and Cell Survival

(A and B) SOCE-induced $[Ca^{2+}]_c$ (A: Fura2 after calibration in μM) and $[Ca^{2+}]_m$ (B: mt-Cepia) time courses in WT and MICU1-KO HEKs expressing the indicated MICU1 constructs, after addition of 3 mM $CaCl_2$.

(C) Bar graph shows $[Ca^{2+}]_m$ response at 60 s, normalized to MICU1-KO HEK response, from data in (B).

(D) $[Ca^{2+}]_m$ plotted against $[Ca^{2+}]_c$ in individual cells.

(E) Measurements of $[Ca^{2+}]_c$ required to reach 1.2 $[Ca^{2+}]_m$ based on data from (D). Mean ± SEM, n = 4–7, *p < 0.05 versus WT, one-way ANOVA.

(F) Representative traces of $[Ca^{2+}]_c$ measured by fura-ff-AM in intact HEKs after an addition of 10 mM $CaCl_2$ and in the presence of 100 μM H_2O_2.

(G) Quantification of the increase in $[Ca^{2+}]_c$ from data in (F) (50 min–10 min).

(H) Quantification of the mitochondrial GSSG/GSH ratio using the mtGrx1-RoGFP2 sensor in the same conditions as in (F).

Mean ± SEM, n = 3 independent experiments, *p < 0.05 versus MICU1-KO, one-way ANOVA.

See also Figures S3 and S4.

a significantly higher inhibition of mitochondrial Ca^{2+} uptake by 30 nM RuRed was obtained in MICU1-KO HEKs rescued with empty vector or MICU1-ΔDID compared to either WT MICU1 or MICU1-EF1-D9E rescue (Figure 4B). Importantly, rescuing MICU1-KO HEKs by the MICU1-ΔDID or MICU1-EF1-D9E constructs both lead to a higher MICU1 protein expression than that in the WT HEKs (Figure S4B). Because no release of any of the MICU1 constructs was noticed upon selective permeabilization of the plasma membrane and in the immunofluorescence experiments, the expressed MICU1 constructs co-localized with the mitochondria (Figure S4C), they seem to be correctly targeted to the mitochondria. To test the localization to the IMS and proper interaction with EMRE for both MICU1-HA and MICU1-ΔDID-HA, we performed for the revision an immunoprecipitation experiment. Figure S4D shows that EMRE (tagged with Myc) pulled down a comparable amount of WT MICU1 and MICU1-ΔDID mutant (tagged with HA), thus confirming the proper localization of the MICU1-ΔDID construct in the IMS and also that alteration of the MICU1-MCU interaction does not interfere with the MICU1-EMRE binding. Furthermore, the dominant-negative effect of MICU1-ΔDID (Figures S3A and S3B) also provides functional evidence for the correct localization of MICU1-ΔDID. Thus, the failure of the DID mutant to restore the lower RuRed sensitivity confirms that the interaction between the DID of MICU1 and MCU, likely through its DIME domain, controls the Ca^{2+} flux and the RuRed sensitivity of the MCU complex.

DISCUSSION

The main finding of this study is that MICU1 interacts with the DIME motif of MCU and this interaction is required for keeping MCU complex's pore both closed at low $[Ca^{2+}]_c$ and optimally activated at high $[Ca^{2+}]_c$. Furthermore, this interaction also

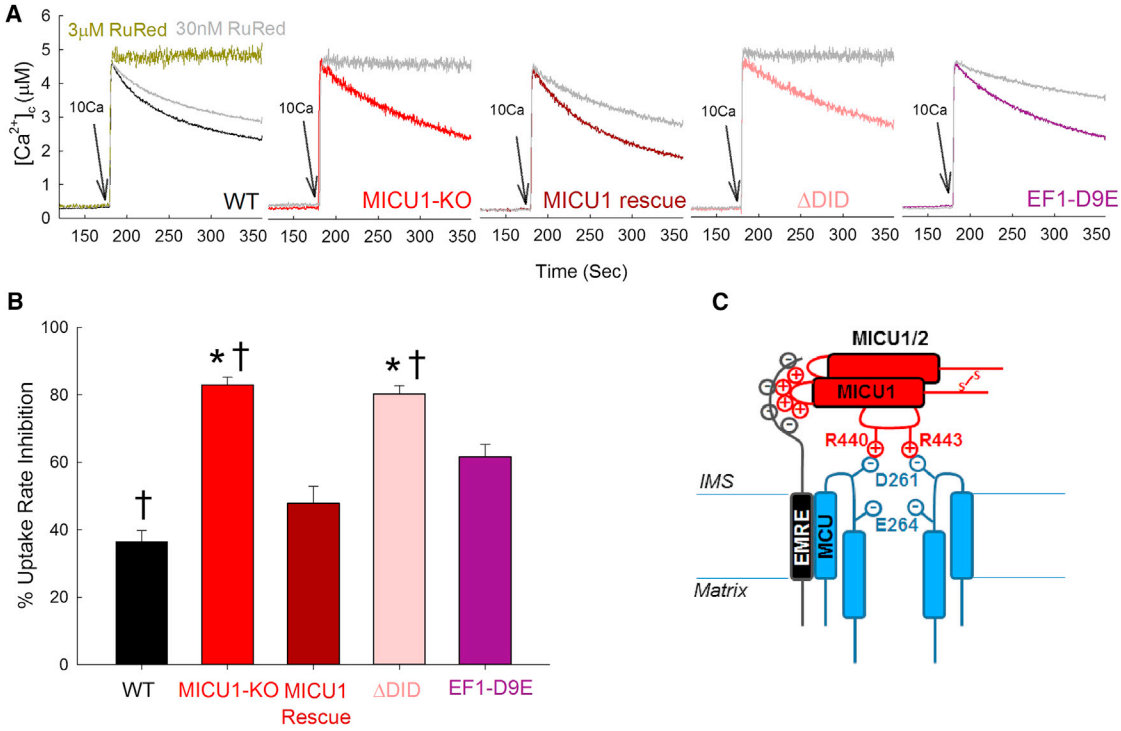

Figure 4. MICU1-MCU Interaction through the DID of MICU1 Is Required to Maintain RuRed Sensitivity

(A) Time courses of the mitochondrial clearance of the $[Ca^{2+}]_c$ rise upon addition of a 10 μM $CaCl_2$ bolus (10Ca) in permeabilized WT and MICU1-KO HEKs with different MICU1 constructs, with or without RuRed (3 μM or 30 nM).

(B) Bar graph shows percentage of uptake rate inhibition by 30 nM RuRed in data from (A). Mean ± SEM, n = 3, *p < 0.05 versus WT, † p < 0.05 versus MICU1-EF1-D9E, one-way ANOVA.

(C) Proposed model for MICU1 interaction with the MCU complex. In addition to the previously identified sites of MICU1 interaction with MICU1/2 through a disulfide bridge and with EMRE via electrostatic binding, we have identified a new functional domain in MICU1, the DID, for interaction with the DIME domain of MCU. More precisely, the two arginines 440 and 443 in MICU1 would interact via salt bridges with the accessible D-ring of the filter selectivity domain of MCU to control the Ca^{2+} flux and RuRed sensitivity of the MCU complex.

See also Figure S4.

controls the MCU complex's accessibility for its most-characterized inhibitors. Thus, our findings are central to understanding the mechanisms that allow MICU1 to support cell survival by preventing mitochondrial Ca^{2+} overload and cause human disease in MICU1 deficiency, and provide important clues for mitochondrial drug development.

It has been broadly recognized that the Ca^{2+}-sensing MICU1 is required for the control of MCU complex activity. As to the underlying mechanism, MICU1's interactions with some components of the MCU complex have been dissected recently: disulfide bonds between the cysteines of MICU1 and MICU2 to form dimers (Patron et al., 2014; Petrungaro et al., 2015) and electrostatic interaction between the polyaspartate tail of EMRE and the polybasic sequence of MICU1 (Tsai et al., 2016). While Hoffman et al. had suggested a potential interaction between the N-terminal polybasic domain of MICU1 and the two interacting coiled-coil domains of MCU (Hoffman et al., 2013), this was later demonstrated to be indirect and mediated through EMRE (Tsai et al., 2016). MICU1's interaction with MCU without EMRE was also indicated (Kovács-Bogdán et al., 2014; Tsai et al., 2016), but until now no direct interaction sites between MCU and MICU1 have been established. Given the involvement of the MCU complex, and specifically MICU1, in cell death and in diseases (Liu et al., 2017; Mammucari et al., 2017), a better understanding of the MICU1 interactions in the MCU complex was clearly needed.

We here report a structural and functional interaction between the DID of MICU1 and the region identified as the selectivity filter domain of MCU, which controls the Ca^{2+} flux and the RuRed sensitivity of the MCU complex. Using sequence alignment, we identified a putative DIME interacting domain, DID, in the C terminus of MICU1, engaging R440 and R443 in potential salt bridges with the D-ring of MCU. Decreased co-immunoprecipitation between MCU and a MICU1 mutant of these two arginines (MICU1-ΔDID: 440KQRLMR445 > 440AQALMA445) supported a structural role for the DID in MICU1-MCU interaction. Using Ca^{2+} imaging approaches in genetically rescued MICU1-KO MEFs and HEKs, we showed that the DID in MICU1 is required for both the threshold and cooperative activation of the MCU complex-mediated Ca^{2+} uptake. Furthermore, the DID was required to avoid mitochondrial Ca^{2+} overload, ROS dysregulation, and the ensuing cell injury. Additionally, unlike MICU1, MICU1-ΔDID expression in MICU1-KO HEKs did not decrease the RuRed sensitivity. Based on the

proposed *in vitro* architecture of MCU as a pentamer (Oxenoid et al., 2016) and on our identification of the MICU1 DID interaction site with MCU, we here propose an updated model of the interactions of MICU1 within the MCU complex (Figure 4C): the two arginines R440 and R443 from one MICU1 would interact with the exposed D-ring (D261) of two MCU units from the pentamer to assure the physiological gatekeeping of the pore. In such a model, however, it would be predicted that only one MICU1 dimer is required to block a pentameric MCU complex. Nevertheless, the pentameric assembly was established *in vitro* using *C. elegans* MCU that lacked the N-terminal 165 amino acids (Oxenoid et al., 2016), and the *in vivo* MCU stoichiometry is yet to be determined. Some earlier studies, based on biochemical data, proposed tetrameric stoichiometry (Raffaello et al., 2013), in which case our model would be compatible with a pair of DID domains (in 2 MICU1 dimers) being able to fully engage with the D-ring of the MCU selectivity filter. Thus, elucidation of the *in vivo* architecture of MCU will be crucial to better appreciate the stoichiometry between MICU1 and MCU per MCU complex.

As to the relevance of the interactions with the different MCU complex components, our results identify the MICU1 interaction with MCU via its DID to be critical for the gatekeeping. In our experiments, relevance of EMRE and dimer formation is also confirmed, but the MICU1-EMRE interaction rather appears as an additional stabilizing interaction to support the tight regulation of MCU by MICU1, which also fits with the only partial loss of threshold observed by Tsai et al. when disrupting the MICU1-EMRE interaction (Tsai et al., 2016). Notably, direct control of MCU by MICU1 as an evolutionarily conserved critical factor in gatekeeping is supported by the finding that the functional MCU complex of *Dictyostelium discoideum* consists of only MCU and one MICU isoform (Kovács-Bogdán et al., 2014).

Our alignment of MICUs suggests that the DID, comprising the two arginines, is conserved among the three MICUs. However, MICU2 fails to act as a gatekeeper in the absence of MICU1 (Kamer and Mootha, 2014). Because some interactions remained between MICU1-ΔDID and MCU (Figure 2B), we speculate that those interactions might be different for MICU1 and MICU2. Thus, further studies will be required to test whether the DID of MICU2 (or MICU3) can support an interaction with MCU.

One of the most unexpected findings of this work was that removal of MICU1 greatly sensitized mitochondria toward RuRed/Ru360, and this seems to be because of the DID limiting access of RuRed to its target site in the DIME of MCU. In the light of recent demonstration of tissue-specific differences in the MICU1 abundance relative to MCU (Paillard et al., 2017), the present finding might predict different RuRed/Ru360 sensitivity of MCU complex in various tissues, such as the particularly high sensitivity in the little MICU1-containing cardiac muscle (Matlib et al., 1998). Furthermore, pharmacological targeting of the MCU complex by new and potentially therapeutically useful molecules has become an area of concerted research efforts (Arduino et al., 2017; Arduino and Perocchi, 2018). Our findings might aid drug design and call attention to possible organ-specific differences in the sensitivity to future drugs sharing the target of RuRed/Ru360.

STAR★METHODS

Detailed methods are provided in the online version of this paper and include the following:

- KEY RESOURCES TABLE
- CONTACT FOR REAGENT AND RESOURCE SHARING
- EXPERIMENTAL MODEL AND SUBJECT DETAILS
  - Cell lines
  - Primary mouse hepatocytes
- METHOD DETAILS
  - Measurements of mitochondrial Ca^{2+} uptake and membrane potential
  - Construction of the HA-tagged MICU1 mutants
  - Co-immunoprecipitation
  - Live cell Ca^{2+} imaging
- QUANTIFICATION AND STATISTICAL ANALYSIS

SUPPLEMENTAL INFORMATION

Supplemental Information includes four figures and can be found with this article online at https://doi.org/10.1016/j.molcel.2018.09.008.

ACKNOWLEDGMENTS

M.P. was a recipient of postdoctoral fellowships from La Fondation pour la Recherche Médicale (FRM SPE20130326561) and American Heart Association (14POST19830021) and a grant "Aide à la mobilité" from the Institut Servier (France). The study was funded by an NIH grant (RO1 GM102724) to G.H.

AUTHOR CONTRIBUTIONS

Conceptualization: G.H., G.C., S.K.J., and M.P.; Investigation: G.H., G.C., S.K.J., M.P., K.-T.H., and P.V.; Writing: G.H., G.C., S.K.J., and M.P.; Funding Acquisition: G.H., M.P.

DECLARATION OF INTERESTS

The authors declare no competing interests.

Received: February 28, 2018
Revised: July 20, 2018
Accepted: September 6, 2018
Published: October 25, 2018

REFERENCES

Antony, A.N., Paillard, M., Moffat, C., Juskeviciute, E., Correnti, J., Bolon, B., Rubin, E., Csordás, G., Seifert, E.L., Hoek, J.B., and Hajnóczky, G. (2016). MICU1 regulation of mitochondrial Ca(2+) uptake dictates survival and tissue regeneration. Nat. Commun. *7*, 10955.

Arduino, D.M., and Perocchi, F. (2018). Pharmacological modulation of mitochondrial calcium homeostasis. J. Physiol. *596*, 2717–2733.

Arduino, D.M., Wettmarshausen, J., Vais, H., Navas-Navarro, P., Cheng, Y., Leimpek, A., Ma, Z., Delrio-Lorenzo, A., Giordano, A., Garcia-Perez, C., et al. (2017). Systematic Identification of MCU Modulators by Orthogonal Interspecies Chemical Screening. Mol. Cell *67*, 711–723.e7, e717.

Baughman, J.M., Perocchi, F., Girgis, H.S., Plovanich, M., Belcher-Timme, C.A., Sancak, Y., Bao, X.R., Strittmatter, L., Goldberger, O., Bogorad, R.L., et al. (2011). Integrative genomics identifies MCU as an essential component of the mitochondrial calcium uniporter. Nature *476*, 341–345.

Cao, C., Wang, S., Cui, T., Su, X.C., and Chou, J.J. (2017). Ion and inhibitor binding of the double-ring ion selectivity filter of the mitochondrial calcium uniporter. Proc. Natl. Acad. Sci. USA *114*, E2846–E2851.

Chakraborty, P.K., Mustafi, S.B., Xiong, X., Dwivedi, S.K.D., Nesin, V., Saha, S., Zhang, M., Dhanasekaran, D., Jayaraman, M., Mannel, R., et al. (2017). MICU1 drives glycolysis and chemoresistance in ovarian cancer. Nat. Commun. *8*, 14634.

Csordás, G., Golenár, T., Seifert, E.L., Kamer, K.J., Sancak, Y., Perocchi, F., Moffat, C., Weaver, D., de la Fuente Perez, S., Bogorad, R., et al. (2013). MICU1 controls both the threshold and cooperative activation of the mitochondrial Ca^{2+} uniporter. Cell Metab. *17*, 976–987.

Gutscher, M., Pauleau, A.L., Marty, L., Brach, T., Wabnitz, G.H., Samstag, Y., Meyer, A.J., and Dick, T.P. (2008). Real-time imaging of the intracellular glutathione redox potential. Nat. Methods *5*, 553–559.

Hoffman, N.E., Chandramoorthy, H.C., Shamugapriya, S., Zhang, X., Rajan, S., Mallilankaraman, K., Gandhirajan, R.K., Vagnozzi, R.J., Ferrer, L.M., Sreekrishnanilayam, K., et al. (2013). MICU1 motifs define mitochondrial calcium uniporter binding and activity. Cell Rep. *5*, 1576–1588.

Ji, L., Liu, F., Jing, Z., Huang, Q., Zhao, Y., Cao, H., Li, J., Yin, C., Xing, J., and Li, F. (2017). MICU1 Alleviates Diabetic Cardiomyopathy Through Mitochondrial Ca^{2+}-Dependent Antioxidant Response. Diabetes *66*, 1586–1600.

Kamer, K.J., and Mootha, V.K. (2014). MICU1 and MICU2 play nonredundant roles in the regulation of the mitochondrial calcium uniporter. EMBO Rep. *15*, 299–307.

Kamer, K.J., Grabarek, Z., and Mootha, V.K. (2017). High-affinity cooperative Ca^{2+} binding by MICU1-MICU2 serves as an on-off switch for the uniporter. EMBO Rep. *18*, 1397–1411.

Kovács-Bogdán, E., Sancak, Y., Kamer, K.J., Plovanich, M., Jambhekar, A., Huber, R.J., Myre, M.A., Blower, M.D., and Mootha, V.K. (2014). Reconstitution of the mitochondrial calcium uniporter in yeast. Proc. Natl. Acad. Sci. USA *111*, 8985–8990.

Lewis-Smith, D., Kamer, K.J., Griffin, H., Childs, A.M., Pysden, K., Titov, D., Duff, J., Pyle, A., Taylor, R.W., Yu-Wai-Man, P., et al. (2016). Homozygous deletion in MICU1 presenting with fatigue and lethargy in childhood. Neurol Genet *2*, e59.

Liu, J.C., Liu, J., Holmström, K.M., Menazza, S., Parks, R.J., Fergusson, M.M., Yu, Z.X., Springer, D.A., Halsey, C., Liu, C., et al. (2016). MICU1 Serves as a Molecular Gatekeeper to Prevent In Vivo Mitochondrial Calcium Overload. Cell Rep. *16*, 1561–1573.

Liu, J.C., Parks, R.J., Liu, J., Stares, J., Rovira, I.I., Murphy, E., and Finkel, T. (2017). The In Vivo Biology of the Mitochondrial Calcium Uniporter. Adv. Exp. Med. Biol. *982*, 49–63.

Logan, C.V., Szabadkai, G., Sharpe, J.A., Parry, D.A., Torelli, S., Childs, A.M., Kriek, M., Phadke, R., Johnson, C.A., Roberts, N.Y., et al.; UK10K Consortium (2014). Loss-of-function mutations in MICU1 cause a brain and muscle disorder linked to primary alterations in mitochondrial calcium signaling. Nat. Genet. *46*, 188–193.

Mallilankaraman, K., Doonan, P., Cárdenas, C., Chandramoorthy, H.C., Müller, M., Miller, R., Hoffman, N.E., Gandhirajan, R.K., Molgó, J., Birnbaum, M.J., et al. (2012). MICU1 is an essential gatekeeper for MCU-mediated mitochondrial Ca(2+) uptake that regulates cell survival. Cell *151*, 630–644.

Mammucari, C., Gherardi, G., and Rizzuto, R. (2017). Structure, Activity Regulation, and Role of the Mitochondrial Calcium Uniporter in Health and Disease. Front. Oncol. *7*, 139.

Matlib, M.A., Zhou, Z., Knight, S., Ahmed, S., Choi, K.M., Krause-Bauer, J., Phillips, R., Altschuld, R., Katsube, Y., Sperelakis, N., and Bers, D.M. (1998). Oxygen-bridged dinuclear ruthenium amine complex specifically inhibits Ca2+ uptake into mitochondria in vitro and in situ in single cardiac myocytes. J. Biol. Chem. *273*, 10223–10231.

O-Uchi, J., Jhun, B.S., Xu, S., Hurst, S., Raffaello, A., Liu, X., Yi, B., Zhang, H., Gross, P., Mishra, J., et al. (2014). Adrenergic signaling regulates mitochondrial Ca2+ uptake through Pyk2-dependent tyrosine phosphorylation of the mitochondrial Ca2+ uniporter. Antioxid. Redox Signal. *21*, 863–879.

Oxenoid, K., Dong, Y., Cao, C., Cui, T., Sancak, Y., Markhard, A.L., Grabarek, Z., Kong, L., Liu, Z., Ouyang, B., et al. (2016). Architecture of the mitochondrial calcium uniporter. Nature *533*, 269–273.

Paillard, M., Csordás, G., Szanda, G., Golenár, T., Debattisti, V., Bartok, A., Wang, N., Moffat, C., Seifert, E.L., Spät, A., and Hajnóczky, G. (2017). Tissue-Specific Mitochondrial Decoding of Cytoplasmic Ca^{2+} Signals Is Controlled by the Stoichiometry of MICU1/2 and MCU. Cell Rep. *18*, 2291–2300.

Patron, M., Checchetto, V., Raffaello, A., Teardo, E., Vecellio Reane, D., Mantoan, M., Granatiero, V., Szabò, I., De Stefani, D., and Rizzuto, R. (2014). MICU1 and MICU2 finely tune the mitochondrial Ca2+ uniporter by exerting opposite effects on MCU activity. Mol. Cell *53*, 726–737.

Petrungaro, C., Zimmermann, K.M., Küttner, V., Fischer, M., Dengjel, J., Bogeski, I., and Riemer, J. (2015). The Ca(2+)-Dependent Release of the Mia40-Induced MICU1-MICU2 Dimer from MCU Regulates Mitochondrial Ca(2+) Uptake. Cell Metab. *22*, 721–733.

Plovanich, M., Bogorad, R.L., Sancak, Y., Kamer, K.J., Strittmatter, L., Li, A.A., Girgis, H.S., Kuchimanchi, S., De Groot, J., Speciner, L., et al. (2013). MICU2, a paralog of MICU1, resides within the mitochondrial uniporter complex to regulate calcium handling. PLoS ONE *8*, e55785.

Raffaello, A., De Stefani, D., Sabbadin, D., Teardo, E., Merli, G., Picard, A., Checchetto, V., Moro, S., Szabò, I., and Rizzuto, R. (2013). The mitochondrial calcium uniporter is a multimer that can include a dominant-negative pore-forming subunit. EMBO J. *32*, 2362–2376.

Sancak, Y., Markhard, A.L., Kitami, T., Kovács-Bogdán, E., Kamer, K.J., Udeshi, N.D., Carr, S.A., Chaudhuri, D., Clapham, D.E., Li, A.A., et al. (2013). EMRE is an essential component of the mitochondrial calcium uniporter complex. Science *342*, 1379–1382.

Tsai, M.F., Phillips, C.B., Ranaghan, M., Tsai, C.W., Wu, Y., Willliams, C., and Miller, C. (2016). Dual functions of a small regulatory subunit in the mitochondrial calcium uniporter complex. eLife *5*, 5.

Vecellio Reane, D., Vallese, F., Checchetto, V., Acquasaliente, L., Butera, G., De Filippis, V., Szabò, I., Zanotti, G., Rizzuto, R., and Raffaello, A. (2016). A MICU1 Splice Variant Confers High Sensitivity to the Mitochondrial Ca^{2+} Uptake Machinery of Skeletal Muscle. Mol. Cell *64*, 760–773.

Wang, L., Yang, X., Li, S., Wang, Z., Liu, Y., Feng, J., Zhu, Y., and Shen, Y. (2014). Structural and mechanistic insights into MICU1 regulation of mitochondrial calcium uptake. EMBO J. *33*, 594–604.

Xue, Q., Pei, H., Liu, Q., Zhao, M., Sun, J., Gao, E., Ma, X., and Tao, L. (2017). MICU1 protects against myocardial ischemia/reperfusion injury and its control by the importer receptor Tom70. Cell Death Dis. *8*, e2923.

STAR★METHODS

KEY RESOURCES TABLE

REAGENT or RESOURCE	SOURCE	IDENTIFIER
Antibodies		
Rabbit anti-MICU1	Sigma-Aldrich	HPA037480; RRID: AB_10696934
Rabbit anti-MCU	Sigma-Aldrich	HPA016480; RRID: AB_2071893
Rabbit anti-MICU2	Abcam	ab101465; RRID: AB_10711219
Mouse anti-mtHsp70	Thermo Fisher	MA3-028; RRID: AB_325474
Rabbit anti-prohibitin	Abcam	ab28172; RRID: AB_777457
Anti-HA polyclonal	Invitrogen	71-5500; RRID: AB_2533988
Anti-FLAG M2	Sigma-Aldrich	F1804; RRID: AB_262044
Anti-Myc monoclonal	Precision	AG10004
Chemicals, Peptides, and Recombinant Proteins		
Anti-DYKDDDDK (FLAG) beads	Genscript	A00187-200
Ruthenium Red	Sigma	R2751
Fura-2 (AM)	Teflabs	0-103
Fura-2 (salt)	Teflabs	0-104
Fura-2 low affinity (AM)	Teflabs	0-136
Fura-2 low affinity (salt)	Teflabs	0-137
Thapsigargin	Enzo Life Sciences	BML-PE180-0005
CGP-37157	Enzo Life Sciences	BML-CM119-0005
Lipofectamine 3000	Life Technologies	L3000008
Complete protease inhibitor cocktail (EDTA free)	Roche	11873580001
Protein A Sepharose	Abcam	ab193256
Critical Commercial Assays		
DC Protein Assay	Biorad	5000112
Experimental Models: Cell Lines		
$MICU1^{loxp/loxp}$ MEF	Antony et al., 2016	N/A
$MICU1^{KO/KO}$ MEF	Antony et al., 2016	N/A
MICU1-KO HEK293T	Sancak et al., 2013	N/A
EMRE-KO HEK293T	Sancak et al., 2013	N/A
HEK293T stably overexpressing mouse MCU-FLAG	O-Uchi et al., 2014	N/A
WT HEK293T	Sancak et al., 2013	N/A
Recombinant DNA		
pcDNA-dest40-MICU1-HA	Kamer et al., 2017	N/A
pcDNA3.1-MICU1-C465A-HA	Patron et al., 2014	N/A
pcDNA-dest40-M1-EF1-D9E-HA, M1-ΔDID-HA and M1-ΔEMRE-HA	This paper	N/A
EMRE-Myc	This paper	N/A
Mt-Cepia	This paper	N/A
mtGrx1-RoGFP	This paper	N/A
Software and Algorithms		
Canvas X	N/A	N/A
Endnote	N/A	N/A
SigmaPlot 12.5	N/A	N/A

CONTACT FOR REAGENT AND RESOURCE SHARING

Further information and requests for resources and reagents should be directed to and will be fulfilled by the Lead Contact, Gyorgy Hajnoczky (gyorgy.hajnoczky@jefferson.edu).

EXPERIMENTAL MODEL AND SUBJECT DETAILS

Cell lines

Mouse embryonic fibroblasts (MEFs) were isolated by trypsin digestion from e14.5 embryos, using *MICU1*$^{KO/loxP}$ mice (for generation see (Antony et al., 2016)), and then immortalized. MEFs were cultured in DMEM (ATCC 30-2002) supplemented with penicillin, streptomycin at 37°C/5%O_2. MICU1-KO, and EMRE-KO HEKs were kindly provided by Dr Vamsi Mootha and grown as previously described (Sancak et al., 2013) and the stable MCU-Flag HEK by Dr Shey-Shing Sheu. Co-transfection of the control plasmid (pcDNA3-dest40) or the HA-tagged MICU1 constructs with the mitochondrial Ca^{2+} sensor mtCepia or the redox sensor mtGrx1-RoGFP2, was performed in MEFs and HEKs using Lipofectamine 3000 according to manufacturers' protocol. Co-transection efficiency was confirmed by immunofluorescence via the HA tag (data not shown). Since a 4-fold higher expression was observed for the WT MICU1-HA construct compared to the other MICU1-HA mutants, we used 1/4 of the DNA amount for the WT MICU1-HA plasmid.

Primary mouse hepatocytes

Primary hepatocytes were isolated by *in situ* retrograde perfusion with collagenase as previously described (Csordás et al., 2013), from *MICU1*$^{loxP/loxP}$ male mice 3 weeks after tail vein-injection with an AAV8-TBG-Cre or an AAV8-TBG Null ($1.3x10^{11}$ pfu/mouse) (Penn Vector Core). Only preparations with greater than 90% viability were used for subsequent experiments. Studies were done in accordance with the Thomas Jefferson University institutional review board guidelines.

METHOD DETAILS

Measurements of mitochondrial Ca^{2+} uptake and membrane potential

Saponin-permeabilized hepatocytes (2 millions), MEFs or HEKs (2.4 mg) were resuspended in 1.5 mL of intracellular medium (ICM) containing 120 mM KCl, 10 mM NaCl, 1 mM KH_2PO_4, 20 mM Tris-HEPES at pH 7.2, and supplemented with proteases inhibitors (leupeptin, antipain, pepstatin, 1mg/ml each), 2 mM MgATP, 2 μM thapsigargin and maintained in a stirred thermostated cuvette at 35°C. Assays were performed in presence of 20 μM CGP-37157 and 1 mM succinate using a multiwavelength-excitation dual-wavelength-emission fluorimeter (DeltaRAM, PTI). The extramitochondrial Ca^{2+} concentration $[Ca^{2+}]_c$ was assessed using the ratiometric Ca^{2+} probe Fura2-FA (1.5 μM, Teflabs) or Fura-IoAff (formerly Fura-FF) (1 μM, Teflabs). $\Delta\psi m$ was measured with 1.5 μM TMRM (Invitrogen). Fura and TMRM fluorescence were recorded simultaneously using 340-380 nm excitation and 500 nm emission, and 545 nm excitation and 580 nm emission, respectively. Complete depolarization (maximum de-quench of TMRM fluorescence) was elicited using of the protonophore FCCP (2 μM). Calibration of the Fura signal was carried out at the end of each measurement, adding 1 mM $CaCl_2$, followed by 10 mM EGTA/Tris, pH 8.5.

Construction of the HA-tagged MICU1 mutants

MICU1-EF1-D9E and MICU1-ΔEMRE were generated by site-directed mutagenesis in the cDNA sequence pcDNA-DEST40 containing the wild-type human MICU1 (provided by Vamsi K. Mootha). MICU1-ΔDID was created by inserting the synthetized sequence coding the appropriate mutations (Blue Heron) between the HindII/EcoNI restriction sites. Finally, the sequence resulting the C-terminal HA tag was inserted into each construct between the EcoNI/AgeI restriction sites. All constructs have been sequenced.

Co-immunoprecipitation

For coIP experiments, HEK293 cells were grown in 10cm plates. After 48h post-transfection the plates were lysed in 1ml of a buffer containing 120mM NaCl, 50mM MOPS (pH 7.2), 0.5mM EGTA, 1% 3-[(3-Cholamidopropyl)dimethylammonio]-1-propanesulfonate hydrate (CHAPS) and protease inhibitor cocktail. Two equal aliquots (approximately 0.5mg protein) were immunoprecipitated with either 15μl FLAG-Ab beads or 1μg of HA or Myc antibody with 50μl of Protein A Sepharose (50% slurry).

Live cell Ca^{2+} imaging

First, the cells were pre-incubated in a serum-free extracellular medium (ECM, 120 mM NaCl, 5 mM $NaHCO_3$, 10 mM Na-HEPES, 4.7 mM KCl, 1.2 mM KH_2PO_4, 1.2 mM $MgSO_4$, 2 mM $CaCl_2$, 10 mM glucose, pH7.4) containing 2% BSA. For SOCE experiments, ER stores were depleted by 10 min pretreatment with 2 μM thapsigarginin in Ca^{2+}-free ECM. For permeabilized cells imaging, mitochondrial loading with 4μM Fura-FF AM was performed for 1h at 37°C, in in a serum-free extracellular medium (ECM, 120 mM NaCl, 5 mM NaHCO3, 10 mM Na-HEPES, 4.7 mM KCl, 1.2 mM KH2PO4, 1.2 mM MgSO4, 2 mM CaCl2, 10 mM glucose, pH7.4) containing 2% BSA and 0.012% Pluronic Acid. After plasma membrane permeabilization for 5 min at 37°C with 40μg/ml saponin, cells were

washed once with ICM and then incubated with ICM supplemented with 2 mM MgATP, 2 μM thapsigargin, 2 mM Succinate, 20μM CGP-37157 and 1μM Rhod2-FA. Fluorescence wide field imaging of $[Ca^{2+}]_c$ and $[Ca^{2+}]_m$ was carried out using a ProEMICU1024 EM-CCD (Princeton Instruments), fitted to Leica DMI 6000B inverted epifluorescence microscopes as previously described (Paillard et al., 2017).

QUANTIFICATION AND STATISTICAL ANALYSIS

Data are expressed as mean ± SEM. Experiments were performed at least 3 times, in duplicates or more. Statistical analysis was performed using ANOVA-1 followed by a Dunn's post hoc test for comparisons between multiple groups.